Subramani, D. N., P. F. J. Lermusiaux, P.J. Haley, Jr., C. Mirabito, S. Jana, C. S. Kulkarni, A. Girard, D. Wickman, J. Edwards, J. Smith, 2017. Time-Optimal Path Planning: Real-Time Sea Exercises. In: Oceans '17 MTS/IEEE Aberdeen, 19-22 June 2017, DOI: 10.1109/OCEANSE.2017.8084776

Time-Optimal Path Planning: Real-Time Sea Exercises

Deepak N. Subramani[a], Pierre F. J. Lermusiaux[a], Patrick J. Haley, Jr.[a], Chris Mirabito[a], Sudip Jana[a], Chinmay S. Kulkarni[a], Andrew Girard[b], Diana Wickman[b], Joe Edwards[c], and Josh Smith[c]
[a]Department of Mechanical Engineering, Massachusetts Institute of Technology, Cambridge, MA 02139 Email: pierrel@mit.edu
[b]Woods Hole Oceanographic Institute Woods Hole, MA 02543 Email: agirard@whoi.edu
[c]Lincoln Laboratory Lexington, MA 02421 Email: joe.edwards@ll.mit.edu

***Abstract*—We report the results of sea exercises that demonstrate the real-time capabilities of our fundamental time-optimal path planning theory and software with real ocean vehicles. The exercises were conducted with REMUS 600 Autonomous Underwater Vehicles (AUVs) in the Buzzards Bay and Vineyard Sound Regions on 21 October and 6 December 2016. Two tests were completed: (i) 1-AUV time-optimal tests and (ii) 2-AUV race tests where one AUV followed a time-optimal path and the other a shortest-distance path between the start and finish locations. The time-optimal planning proceeded as follows. We first forecast, in real-time, the physical ocean conditions in the above regions and times utilizing our MSEAS multi-resolution primitive equation ocean modeling system. Next, we planned time-optimal paths for the AUVs using our level-set equations and real-time ocean forecasts, and accounting for operational constraints (e.g. minimum depth). This completed the planning computations performed onboard a research vessel. The forecast optimal paths were then transferred to the AUV operating system and the vehicles were piloted according to the plan. We found that the forecast currents and paths were accurate. In particular, the time-optimal vehicles won the races, even though the local currents and geometric constraints were complex. The details of the results were analyzed off-line after the sea tests.**

I. Introduction

Autonomous underwater vehicles (AUVs) are employed in many applications such as ocean sensing, search and rescue operations, acoustic surveillance, and oil and gas exploration. With advances in AUV capability [1], [2] and increasing mission complexity, there is a demand for predicting all reachable locations, prolonging endurance, and reducing operational costs by optimally utilizing ocean flow forecasts for navigation. For such optimal navigation, we recently developed new theory, schemes, and computational systems for an exact partial differential equation-based path planning [3], [4]. This level-set path planning was applied previously using realistic re-analysis simulations for the sustained coordinated operation of multiple collaborative AUVs for time-, coordination- and energy- optimal missions [5], [6], [7]. In the present paper, our goal is to demonstrate our level-set path planning in real-time sea exercises with real AUVs in shallow coastal ocean regions with strong and dynamic currents, and complex bathymetry and coastlines. We completed these exercises in the Buzzard's Bay and Vineyard Sound regions (Fig. 1) during Oct. to Dec. 2016. Presently, we discuss results from the sea exercises on 21 Oct. 2016 and 06 Dec. 2016. Our specific objectives are to report: *(i)* the improvements to our 4-D primitive equation ocean modeling system for accurately forecasting the currents in the Buzzard's Bay and Vineyard Sound region; *(ii)* the results of the time-optimal path planning of REMUS 600 AUVs using our fundamental theory and real-time forecasts; *(iii)* the portability of our software systems for real-time optimal path prediction in multiple regions and its ability to work with the AUV navigation software.

We note that only a small number of sea trials of optimal path planning have been reported in the literature e.g., [8]. Most path planning aims to follow specific tracks, usually for ocean sections, e.g., [9], [10]. Some laboratory experiments for tracking have been completed, e.g., [11]. More path planning for AUVs with realistic ocean data and simulations have been completed, e.g., [12], [13], [14]. However, most schemes do not solve exact partial differential equations (PDEs) for rigorous optimal path planning. The capability of solving our time-optimal PDEs very quickly such they can be used in real-time onboard a ship for controlling AUV missions is a main achievement of the present work.

The manuscript is organized as follows. In Sec. II, we outline our path planning methodology. In Sec. III, we describe the specific AUVs utilized for the tests, the ocean modeling system employed for forecasting ocean currents in the Buzzards Bay and Vineyard Sound regions, and relevant features of our path planning software. Next, in Sec. IV, we describe the 1-AUV sea-tests on 21 Oct. 2016 and in Sec. V the 2-AUV race-tests completed on 06 Dec. 2016. Finally, we provide conclusions and future outlooks in Sec. VI.

II. Methodology Synopsis

The goal of our path planning is to compute time optimal paths $\mathbf{X}_P^*(\mathbf{x}_s, t)$ of a vehicle P traveling with a nominal speed $F(t)$ from a point $\mathbf{x}_s$ to $\mathbf{x}_f$ in any strong and dynamic ocean currents $\mathbf{v}(\mathbf{x}, t)$ (Fig. 2). Our level-set optimal path planning predicts the evolution of the reachability front of all vehicles P for the specified nominal speed and currents. The reachability front is the level-set defined as the set of points which encompasses all locations that can be reached in a given time. Its dynamics is governed by the following PDE

978-1-5090-5278-3/17/$31.00 ©2017 IEEE

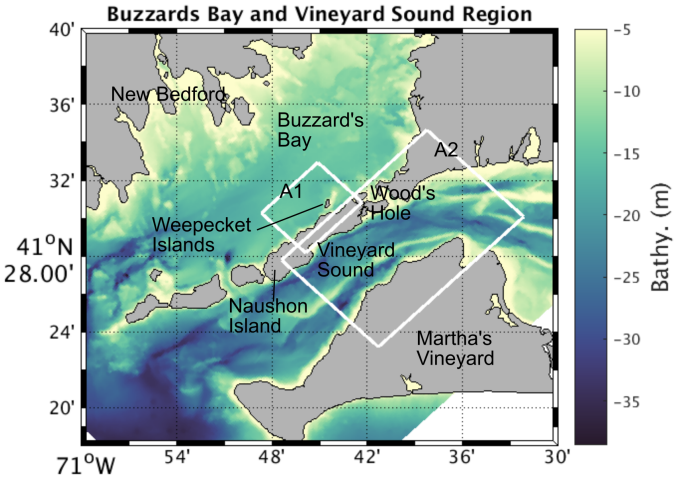

Fig. 1. *Bathymetry and operational areas in the Buzzards Bay and Vineyard Sound Region*: The bathymetry (in m) of the region is shown on the color axis. The domain is discretized with 100 m resolution horizontally and 12 optimized vertical levels.

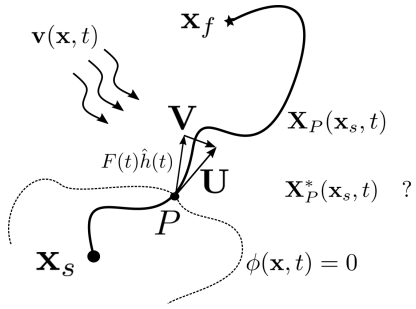

Fig. 2. *Schematic of time-optimal path planning*: We compute and utilize the time-optimal trajectory $\mathbf{X}^*_P(\mathbf{x}_s,t)$ for a vehicle P traveling with a nominal speed $F(t)$ from a start $\mathbf{x}_s$ to a target $\mathbf{x}_f$ in dynamic ocean currents $\mathbf{v}(\mathbf{x},t)$. The effective velocity $\mathbf{U}$ of P at any point is the vector sum of the background flow at that point $\mathbf{V}$ and the forward thrust $F(t)\hat{h}(t)$, i.e., $\mathbf{U}=\mathbf{V}+F(t)\hat{h}(t)$. $\phi(\mathbf{x},t)=0$, is the zero level-set contour which defines the reachability front for P, governed by eq. 1.

for $\phi(\mathbf{x},t)$,

$$\frac{\partial\phi(\mathbf{x},t)}{\partial t}+F(t)|\nabla\phi(\mathbf{x},t)|+\mathbf{v}(\mathbf{x},t)\cdot\nabla\phi=0\,, \qquad (1)$$

with an initial condition $\phi(\mathbf{x},0)=|\mathbf{x}-\mathbf{x}_s|$ and open boundary conditions. The zero level-set contour of the solution $\phi(\mathbf{x},t)$ of the above PDE eq. (1) at any given time $t>0$ is the reachability front of a vehicle starting from $\mathbf{x}_s$ at $t=0$. We have shown that the reachability front tracks all the points that the vehicle can possibly reach at any given time. Its evolution contains all the time-optimal paths of P to any target starting from $\mathbf{x}_s$. The optimal arrival time at the target $\mathbf{x}_f$ starting from $\mathbf{x}_s$, $T^*(\mathbf{x}_f;\mathbf{x}_s)$, is the first time t for which $\phi(\mathbf{x_f},t)=0$. The exact time-optimal paths $\mathbf{X}^*_P(\mathbf{x_s},t)$ are then extracted from the time history of the reachability front, using the particle backtracking equation (when and where ϕ is differentiable),

$$\frac{\mathrm{d}\mathbf{X}^*_P(\mathbf{x}_s,t)}{\mathrm{d}t}=-\mathbf{v}(\mathbf{X}^*_P(\mathbf{x}_s,t),t)-F(t)\frac{\nabla\phi(\mathbf{X}^*_P(\mathbf{x}_s,t),t)}{|\nabla\phi(\mathbf{X}^*_P(\mathbf{x}_s,t),t)|}\,,$$
$$\mathbf{X}^*_P(\mathbf{x}_s,,T^*(\mathbf{x}_f;\mathbf{x}_s))=\mathbf{x}_f\,. \qquad (2)$$

To forecast optimal paths $\mathbf{X}^*_P(\mathbf{x_s},t)$ in the ocean, we need the current forecasts $\mathbf{v}(\mathbf{x},t)$, the vehicle speed $F(t)$, and the sets of start $\mathbf{x}_s$ and end points $\mathbf{x}_f$. For current forecasts, we utilize our data-driven 4-D primitive equation ocean modeling system (MSEAS [15], [16]) forced by high-resolution tidal and real-time atmopsheric forcing fields. For vehicle speeds, we vary the thruster RPM and choose stable operational speeds. To identify interesting paths, we employ a broad search which simulates both time-optimal AUVs and non-optimal AUVs for many start and end points, accounting for the operational constraints. From the several options, a few were selected based on considerations of safe launch and recovery. The computed time-optimal paths are transferred to the AUV operating system in the required format.

III. Ocean Vehicles, Real-Time Ocean Forecasts and Planning Software

A. REMUS 600 Autonomous Underwater Vehicle

The specific AUVs utilized for the present sea exercises were the Hydroid REMUS 600 vehicles. The REMUS 600 is a versatile vehicle with a modular design that enables easy mission specific reconfigurations [17], [18]. When fully charged, it has a mission endurance of nearly 70 hours with speeds up to 5 knots at depths up to 600 meters [19], [20]. The REMUS 600 was launched and recovered from the *R/V Discovery*. For the missions, the REMUS was configured to follow way-points provided to it from our path planning software. The AUVs were operated at 3 m depth at several thruster RPM settings to allow for different vehicle speeds. Fig. 3 shows four photographs from our first sea exercise. In Fig. 3a, the REMUS 600 is being loaded to the *R/V Discovery*. Fig. 3b shows the MIT, WHOI and Lincoln teams utilizing our path planning software to compute time-optimal paths for the REUMS 600 on laptops on board the *R/V Discovery*. Fig. 3b shows a screen shot of the REMUS 600 Vehicle Interface Program, and Fig. 3d shows the REMUS 600 before it dives for a mission.

B. PE Model for Synoptic Ocean Forecasting

To accurately predict the currents in the shallow Buzzard's Bay and Vineyard Sound region (Fig. 1), we employ the MSEAS nonlinear free-surface hydrostatic primitive-equation (PE) modeling system. Two smaller domains are shown in Fig. 1, overlaid on bathymetry. In the horizontal, the grid resolution is 100 m, and in the vertical, 12 generalized-level vertical-coordinates are employed. The model is initialized with objectively-analyzed temperature and salinity climatological fields, very limited recent ocean data, and PE balanced velocity fields. Barotropic tides based on the 1/30 deg resolution TPXO8-ATLAS surface-tide velocities and elevation [21] are used as input to a higher-resolution

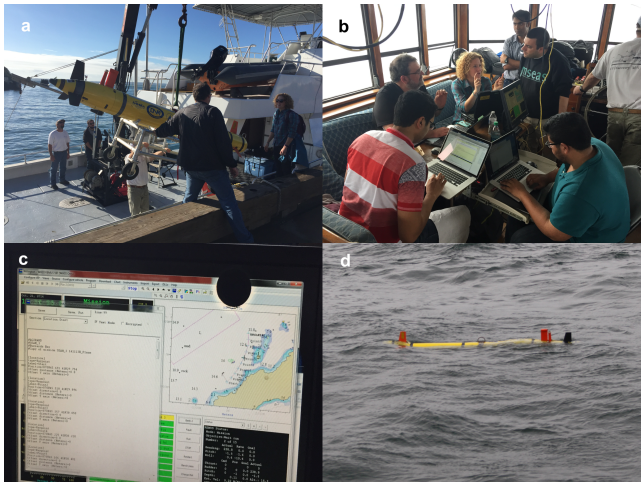

Fig. 3. *Sea Experiments:* **(a)** Loading the REMUS 600 onto the R/V Discovery; **(b)** MIT, WHOI and Lincoln teams planning missions on board the R/V Discovery; **(c)** Screenshot of the AUV OS and Mission Control; **(d)** REMUS 600 before it dives for one of the missions.

nonlinear inversion, that extends the linear scheme of [22]. Specifically, the TPXO8-ATLAS surface-tides are adjusted to the high resolution bathymetry and to a nonlinear bottom drag parameterization tuned using historical current meter data from NOAA CO-OPS and the WHOI Nantucket Sound Circulation project. The resulting nonlinear tides are then merged with the subtidal initial fields, following [16]. Atmospheric-forcing flux forecasts are applied at the free-surface, using the 5-km and 1-hour resolution forecasts from the Weather Research and Forecasting (WRF) simulations at NCEP. At lateral ocean boundaries, a new mixed sponge-radiation-tide open boundary condition formulation is used [23]. Finally, the numerical and sub-grid-scale parameters were tuned for the region by comparison of many PE simulations with varied historical data. After the first sea exercise, we also noticed that the horizontal coastal boundary layers could be improved. This was accomplished by tuning the sub-grid-scale parameterizations for the barotropic velocities and surface elevation to reduce the effective dissipation near the coasts.

C. Path Planning Software

Our path planning software accepts ocean forecasts and AUV speed as inputs. Forecast fields are first processed to a C-grid on which the level-set eq. 1 and backtrack eq. 2 are solved to forecast time optimal paths. This is a pre-processing step and has to be completed only when new forecasts are available. For spatial discretization, we utilize 2-d conservative finite volumes and for temporal discretization we have implemented forward Euler, fractional time step methods, and other higher order time marching schemes. Several options for computing the advection and thrust ($|\nabla\phi|$) terms in eq. 1 exist: Total Variation Diminishing (TVD) schemes, central difference schemes with Shapiro filtering, and first-order and second-order viscosity solution satisfying schemes. All codes have been vectorized for maximally utilizing in-built parallelization. As such, computation is quick and hundreds of paths for one start location (in a domain of size such as used here) can be computed in less than one minute on a MacBook Pro with Intel Core i5 and 16GB DDR3 RAM. The codes are portable and work equally well with classic operating system.

IV. Sea Exercise on 21 October 2016: 1-AUV Time-Optimal Tests

Our first sea exercise occurred on 21 Oct 2016. The objectives of this exercise were to test the usability of our path planning software in real-time and to evaluate the accuracy of our ocean models and path planning. A single AUV was used and made to follow way-points of time-optimal paths between a start and finish locations. Due to strong winds conditions and high waves in other regions, two missions were completed off the Weepecket Islands: Mission 1 from the southwest to the north along the western shore of the Weepecket Islands, and Mission 2 from offshore on the north to the north shore of Weepecket Islands.

Our current forecast was for 3 days starting from 00 Z, 19 Oct 2016 using the latest atmospheric forecasts available at 12 Z, 20 Oct 2016. Fig. 4 shows the winds from this atmospheric forecast in the computational domain. On 21 Oct, winds in the domain were from southeast. Earlier in the day (13–16Z or 9 am–12 noon EDT), there were winds 12-14 knots in the Vineyard Sound and Buzzards Bay. Between 16–19 Z, winds were 8-10 knots in the leeward side (west and northwest) of the Weepecket Islands. The winds in the next 4 hours (19–22 Z), the main period of our tests, are shown in the four panels of Fig. 4. Winds near the Weepecket Islands are 14-16 knots, increasing away from the coast of Naushon Islands and reaching up to 18 knots in the middle of Buzzards Bay and 20 knots near the coast along New Bedford. At 20 Z, the winds in the Vineyard Sound were 20 knots from the southeast. For the AUV tests, we had initially identified three regions based on a broad search for interesting paths. Based on weather and sea conditions, we decided to work in the area near Weepecket Islands (A1 in Fig. 1) as the leeward side of the islands offered safe sea conditions for the launch and recovery of the AUVs. This also allowed us to show that all of our path planning could be reset in an other region and re-planned in just a few minutes of computation.

The forecast currents at 3 m depth were extracted for the planning horizon 13 Z to 22 Z (i.e., 09 to 18 EDT) and transfered to laptops on board *R/V Discovery*. The 3 m currents in A1 from 19 to 22 Z are shown in Fig. 5. The forecast flow at 3 m depth is towards the south-southeast along the shore of Naushon Island. Near the Weepecket Islands, the flow strength was $\approx$ 15 cm/s and the maximum flow of $\approx$ 25 cm/s was in a region north-northwest of Weepecket at 20 Z. The flow weakened in the next two hours reaching 15-20 cm/s north of the Weepecket Islands. We note that we had completed path planning in an idealization of such a flow behind an island [3], so this test in real conditions had a special character.

In the region A1, we adaptively computed more than 100 optimal paths for multiple start and end points, and start times.

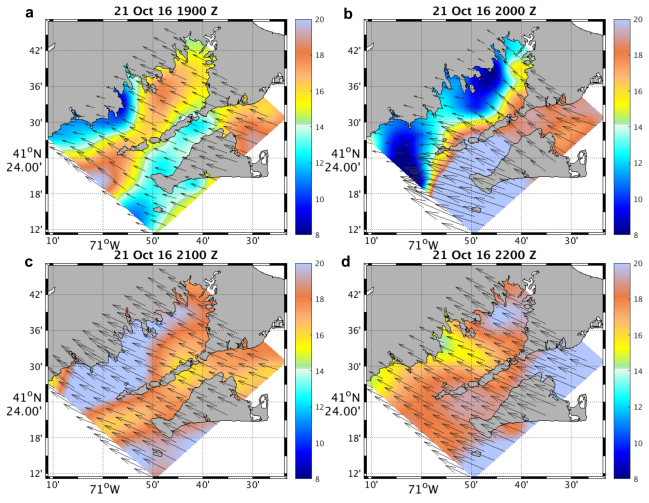

Fig. 4. *Winds in the Buzzard's Bay and Vineyard Sound Regions*: The surface wind vectors are overlaid on a color plot of the speed (in knots). The hourly surface wind forecasts from 19 Z to 22 Z, issued at 12 Z on 20 Oct 2016.

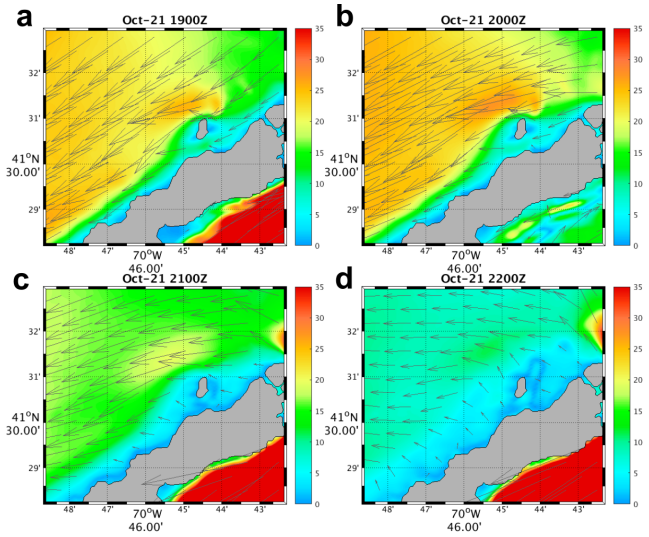

Fig. 5. *Ocean current forecasts around Weepecket Island from the MSEAS PE model* : The horizontal currents at 3 m depth are represented by vectors overlaid on a color plot of the flow magnitude (in cm/s). Forecasts are shown at every hour from 19Z to 22Z (3pm EDT to 6pm EDT) during which we completed our sea tests.

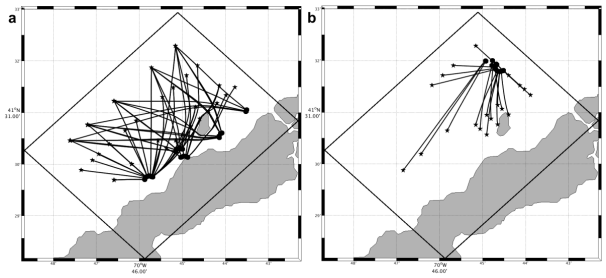

Fig. 6. *Candidate time-optimal paths for missions on 21 Oct. 2016:* More than 100 paths were computed between several start locations (circles) and targets (stars) spread in the region near Weepecket islands: **(a)** Candidates for Mission 1, **(b)** Candidates for Mission 2

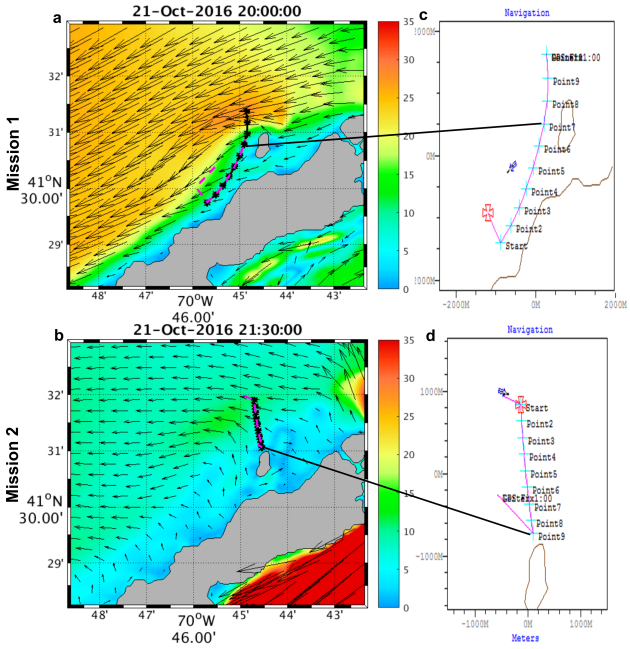

Fig. 7. *Forecast and executed time-optimal paths:* **(a)** Mission 1 - The way-points of the time-optimal path forecast is shown as black markers and the executed path of REMUS 600 is shown by dashed magenta line. On the background, current forecast at 20:00 Z is shown as vectors overlaid on a color map of magnitude; **(b)** Same as (a), but for Mission 2, with current forecast at 21:30 Z; **(c)** The way-point in the AUV mission configuration for Mission 1; **(d)** Same as (c), but for Mission 2.

Fig. 6a shows the paths we first considered for our Mission 1 with start times between 19:00–19:30 Z. For this mission the REMUS 600 was planned to operate at 3 m depth at a nominal speed of 2 knots. We then chose a path for Mission 1 as shown in Fig. 7a, in which the path is overlaid on the forecast of currents at 20 Z. The way-points computed by our path planning software were transferred to the AUV in the required format and the AUV plan obtained is shown in Fig. 7c. The Mission 1 started at 19:24 Z and was completed at 20:25 Z when the AUV OS crashed and the mission had to be aborted after reaching way-point 7 (Fig. 7c). For Mission 1, the predicted travel time to way-point 10 was 95.5 mins and to way-point 7 was 66.85 mins. The actual time to reach that way-point 7 was 61.17 mins. After recovering the AUV, a second mission was planned with path candidates in Fig. 6b. In Fig. 7d, the chosen path for Mission 2 is shown, overlaid on the current forecast at 21:30 Z. Mission 2 started at 21:26 Z and finished at 21:45 Z. The wall clock times, average speeds, distance traveled, travel time and predicted travel time for both missions 1 and 2 are furnished in Table. I. Fig. 3 shows some images from the sea exercise on 21 Oct. 2016. Our travel time predictions were accurate within 10% difference from the actual travel times. This is an excellent result since we had no in-situ synoptic ocean data and the measured nominal speeds of the AUV had larger relative noisy oscillations [24].

Next, we compare the current measured by the ADCP on

TABLE I
21 OCT. 2016 1-AUV TEST TIMINGS

Mission	Path	Wall Clock at Start (Z)	Wall Clock at Stop (Z)	Avg. Nom. Speed (cm/s)	Avg. Eff. Speed (cm/s)	Distance Traveled (km)	Travel Time (mins)	Predicted Time (mins)
1	Time-Optimal	19:24:28	20:25:38	79.24	59.75	2.19	61.17	66.85
2	Time-Optimal	21:26:38	21:45:34	126.75	125.73	1.43	18.95	23

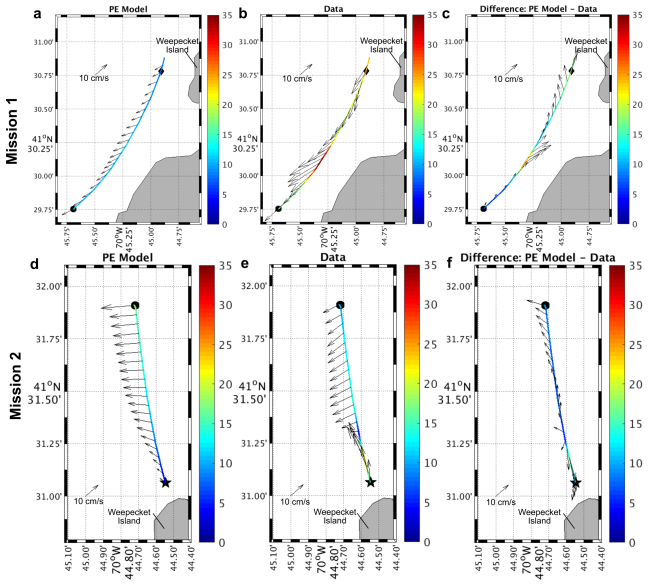

Fig. 8. *Comparison of currents forecast by PE and measured by the AUV on 06 Dec 2016:* **(a)** Magnitude of the flow forecast by the MSEAS PE model along the AUV track is colored, sub-sampled vectors are also shown; **(b)** Magnitude of the flow measured by the AUV is colored, sub-sampled vectors are also shown; **(c)** The difference of the flow magnitude forecast by the MSEAS PE model and measured by the AUV is colored. Sub-sampled vector difference of velocities are also shown. In (a,b,c), the mission's start location is indicated by a circle, and the 7th way-point is indicated by a diamond. **(d,e,f)** Same as (a,b,c), but for Mission 2. Here, the start location is indicated by a circle and the target by a star.

board the REMUS 600 and that predicted by our model. In Fig. 8, we present the comparison over 3 columns. The first column (a,d) shows local current forecasts from our PE model at the times at which the REMUS 600 was present at that location. The second column (b,e) shows the data collected at those locations by the REMUS 600 AUV during its mission. The third column (c,e) shows the difference between our PE model prediction and the data collected. The first row is for Mission 1 and the second row is for Mission 2. Our model was able to predict the direction of currents accurately for both missions. The magnitude of currents near the coast of Naushon Island in Mission 1 was under predicted by the model. This was later diagnosed to be due to the particular subgrid-scale parameters including the Shapiro filtering options utilized in the model run. For our next sea exercise on Dec 06 (Sec. V), these parameters and options were updated. In Fig. 9, we show the time-series of zonal and meridional components of the velocity predicted by the PE model and that measured by the AUV. Fig. 9a and b are for Mission 1 and Fig. 9c and d are for Mission 2.

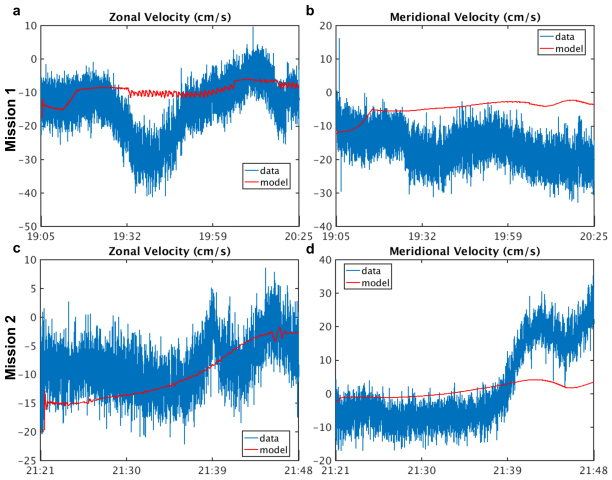

Fig. 9. *Time-series comparison of zonal and meridional components of currents forecast by PE and measured by the AUV on 21 Oct 2016:* **(a)** Zonal component of the horizontal velocity predicted by the PE model is shown by a red line and that measured by the AUV during Mission 1 is shown by the blue line; **(b)** Meridional component of the horizontal velocity predicted by the PE model is shown by a red line and that measured by the AUV Mission 1 is shown by the blue line; **(c,d)** Same as (a,b) but for Mission 2.

V. SEA EXERCISE ON 06 DECEMBER 2016: 2-AUV RACE TESTS

Our second sea exercise took place on 06 Dec 2016. The objective of this exercise was to pilot and compare two identical AUVs in race conditions–one following the computed time-optimal path and the other following a shortest-distance path (or *straight-line* if not blocked by coastlines or minimum depth or ship traffic constraints)-, each with the same start and finish locations. We note that we used the level-set and backtracking equations themselves to compute this *straight-line* path that avoids shallow unsafe operational regions. Of course, these *straight-line* paths are optimized for utilizing currents to reduce travel time. They simply minimize the distance traveled and are exactly computed using the level-set equation with zero propulsion ($F = 0$) and all of the masked or unsafe operational regions that are treated as forbidden regions [3]. The backtracking equation then provides an exact shortest-distance path from the start to the end points that avoids all of the forbidden regions along the way. Overall, a total of 3 missions were completed on 06 Dec, 2016: (1) off Nobska Point; (2) off the northwest coast of Martha's Vineyard along the Middle Ground; and, (3) across northern Vineyard Sound from the Middle Ground to Nobska Point.

Similar to the first sea exercise, our ocean currents forecast was for 3 days starting from 00 Z, 04 Dec 2016 using the latest

atmospheric forecasts available at 12 Z, 05 Dec 2016. From the experience in the first sea exercise, we made minor updates to the options for lateral subgrid-scale numerical schemes in our PE model, as described in III-B.

Fig. 10 shows the winds from this atmospheric forecast in the computational domain. Overall, the winds were weaker on Dec 06 than on Oct 21. Early in the day (14 Z) the winds were out of the north at 16 knots. They slightly weakened over the next hour, decreasing to 14-16 knots in the Buzzard's Bay and Vineyard Sound, with a maximum near Naushon Islands. The winds continued to weaken over the next two hours (down to 11-12 knots by 17 Z) and began to change direction, becoming more northeasterly. For the rest of the day, the winds were out of the northeast and strengthening (13-16 knots by 22 Z). The wind patterns resulted in a favorable sea state for operations.

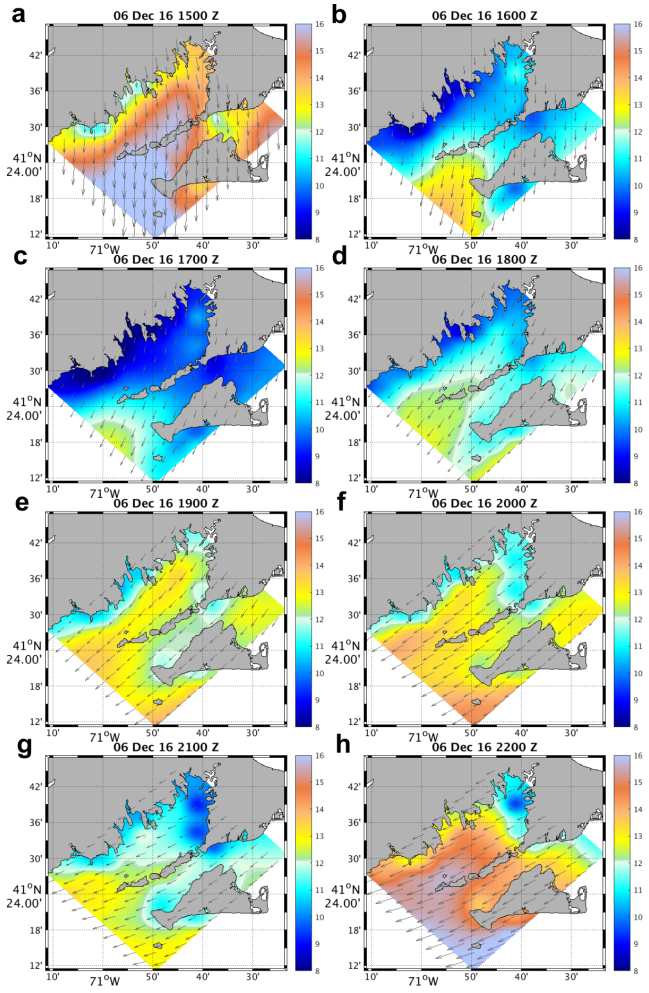

Fig. 10. *Winds in the Buzzard's Bay and Vineyard Sound Regions on 06 Dec. 2016*: The surface wind vectors are overlaid on a color plot of the speed (in knots). The hourly surface wind forecasts from 16 Z to 23 Z, issued at 12 Z on 05 Dec 2016.

Fig. 11 shows the ocean currents at 3 m depth during the main period of the three missions, from 11 am to 6 pm EST. One can clearly observe that the flows are strongly influenced by M2 tidal forcing with complex and rapid modulations of tidal phases and currents by the coastlines, semi-enclosed water bodies, and complex bathymetric features including sand bars and rises such as Middle Ground just northwest of Martha's Vineyard. However, wind-forcing and density-driven flows are not negligible and they modify this surface intensified tidal flow.

In Vineyard Sound, starting at 15 Z the tides are slack and velocities are in the 10-20 cm/s range. Note that the largest flows at Woods Hole and in Buzzards Bay are out of phase with that Vineyard Sound flow. Over the next hour, the tides build a flow to the northeast with typical velocities around 40 cm/s and larger velocities around West Chop and at the exit of Woods Hole (80-100 cm/s). Over the next 2 hours, the tides maintain direction and continue to strengthen, becoming 60-110 cm/s. Shoals in Vineyard Sound introduce smaller scale features and rips, both north of West Chop and in the Middle Ground. The tide weaken over the next three hours, becoming slack again by 21 Z. Then a reverse flow begins to build by 22 Z, with at least 40 cm/s in the entire Sound and larger velocities (70 cm/s) around West Chop and by Nobska Point.

Fig. 12 shows the time-optimal way-points ('*' markers), straight-line way-points ('+' markers), the time-optimal path (magenta dashed line) and straight-line path (blue dotted line) actually followed by the AUV. The background in these plots is the currents at the times shown (roughly the start, mid and end of the missions). The first row is for Mission 1, second for Mission 2 and third for Mission 3.

Table. II shows the wall clock times, avg. speeds, distance traveled, and the travel times for the three missions. The two AUVs used were actually found to be not exactly identical. As a result, their capabilities, most importantly, their average nominal speeds differed ever so slightly. For the third mission, we in fact flipped the AUVs (the one used for the forecast straight-line was used for the forecast fastest path) and this is how we found out that the nominal speed of the two AUVs differed somewhat. Therefore, for fair comparisons, we have to account and correct for this small difference in speeds when estimating travel times. It does not affect the final results, but it is done simply for accuracy. Hence, let the average speeds of the AUVs be F_1 and F_2. If $F_1 > F_2$, then the estimated travel time t_2 is augmented with a revised time as $t_2' = t_2 F_2 / F_1$.

Mission 1 started at 16:27 Z, when the tides were driving a flow to the northeast in the Sound and strengthening. The time-optimal AUV stayed closer to the coast where the forecast opposing currents are weaker compared to the straight-line AUV which gets caught in stronger opposing currents (Fig. 12a,b,c). Here, both vehicles reached the finish location. The travel time of the time-optimal AUV reported in Table. II was complemented with a time revised upwards to account for the slight difference in the start location, and the travel-time for the straight-line AUV was complemented with a time revised downwards to account for its lower avg. nominal speed. After these corrections, the time-optimal AUV took 40.46 mins and straight-line AUV 45.27 mins to complete the same mission. As a result, following our time-optimal path prediction is 10% faster than following a shortest-distance straight-line path.

TABLE II
06 DEC. 2016 2-AUVS-RACE TEST TIMINGS

Mission	Path	Wall Clock at Start (Z)	Wall Clock at Stop (Z)	Avg. Nom. Speed (cm/s)	Avg. Eff. Speed (cm/s)	Distance Traveled (km)	Travel Time* (mins)
1	Time-Optimal	16:27:46	17:08:14	150.88	122.10	2.97	40.46
	Straight-Line	16:27:25	17:18:47	132.97	86.73	2.67	45.27
2	Time-Optimal	18:15:55	19:52:02	153.34	146.06	8.44	96.12
	Straight-Line Restart	18:15:16 18:52:42	18:37:01 20:09:00	148.08	116.93	6.97	110.72
3	Time-Optimal	20:41:05	21:27:47	164.62	165.79	4.64	47.97
	Straight-Line	20:40:06	21:27:54	169.94	175.32	4.94	50.55

*Where applicable, travel time has been corrected for differences in start and finish locations, speeds of the 2 AUVs, and restarts as described in Sec. V.

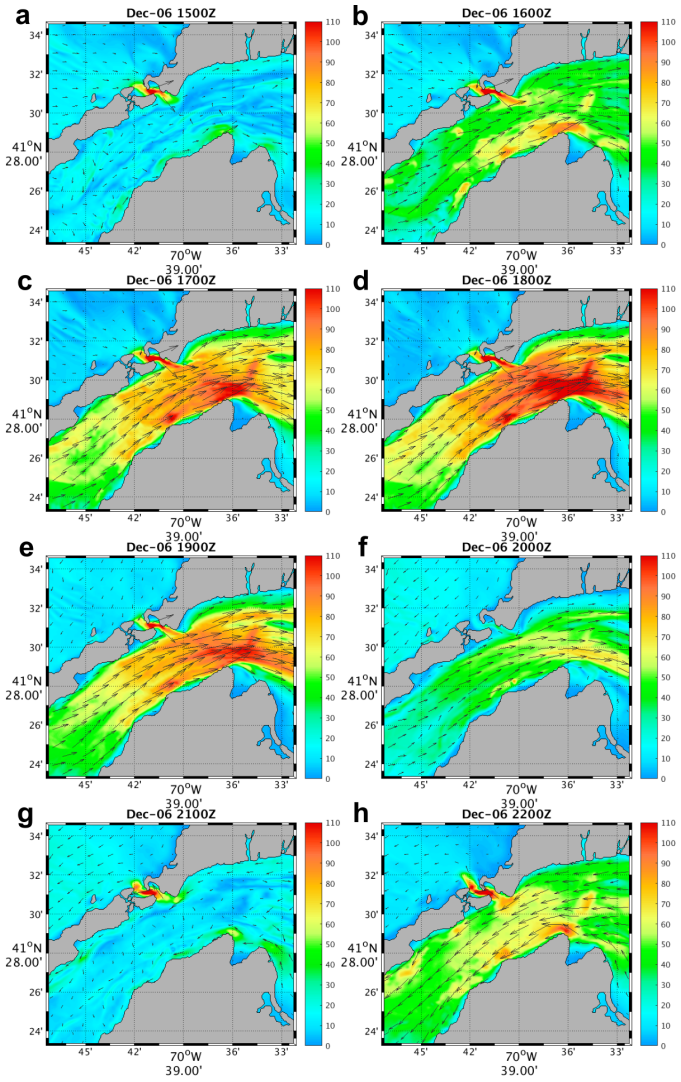

Fig. 11. *Ocean current forecasts in Vineyard Sound issued by the MSEAS PE model on 06 Dec. 2016*: The horizontal currents at 3 m depth are represented by vectors overlaid on a color plot of the flow magnitude (in cm/s). Forecasts are shown at every hour from 16 Z to 23 Z (11 am to 6 pm EST) during which we completed our sea tests.

Mission 2 started at 18:15 Z. The flow was still to the northeast but the tides were slackening. The time-optimal AUV crossed the strong opposing jet and reached a region with weaker opposing flows to continue its journey to the target (Fig. 12d,e,f). On the other hand, the straight-line AUV got caught in opposing flows of up to 110 cm/s and had to abort its mission temporarily. This AUV was restarted and the mission continued. After the time-optimal AUV reached the finish location, the straight-line AUV was allowed to continue to account for the time lost in restarting. Then, when it became clear that the straight-line AUV was nonetheless going to arrive much later than the forecast fastest AUV, the mission was aborted so as to save time for a third mission. At that abort time, the straight-line AUV was still far from the finish location, about 1 km away. The estimate of travel-time was corrected to account for this fact. Here, as a result, the forecast time-optimal AUV took 96.12 mins, about 15% faster than the straight-line AUV, which took 110.72 mins.

Mission 3 started at 20:40 Z. The currents were forecast to be weak when these missions started and to intensify due only towards the end of the mission (Fig. 12g,h,i). This is because of the tidal flow reversal around that time in the Vineyard Sound. We note that that reversal is rapid and complex with local jets (as seen from the Fig. 12g,h,i). It is actually challenging to forecast such transition with a PE modeling system without data. Nonetheless, after accounting for the differences in the AUV speeds, the time-optimal AUV took 47.97 mins and the straight-line AUV took 50.55 mins. Here, using our time-optimal paths results in the AUV being 6% faster than the competing AUV following a straight-line.

Next, in Fig. 13 and Fig. 14, we compare the predictions by our PE model and the data collected by the AUV as in Oct 21 missions (Sec. IV). We see that the improvements we made to our PE modeling system since Oct 21 have helped and the difference in magnitude between the predicted currents and data is now even smaller. Following our time-optimal paths allow AUVs to be 6-15% faster at reaching their targets than a shortest distance path. This is due to the variations in the currents, even though the paths were never more than 1 km apart. Our current forecasts had skill and this allowed us to predict and utilize such current variations successfully.

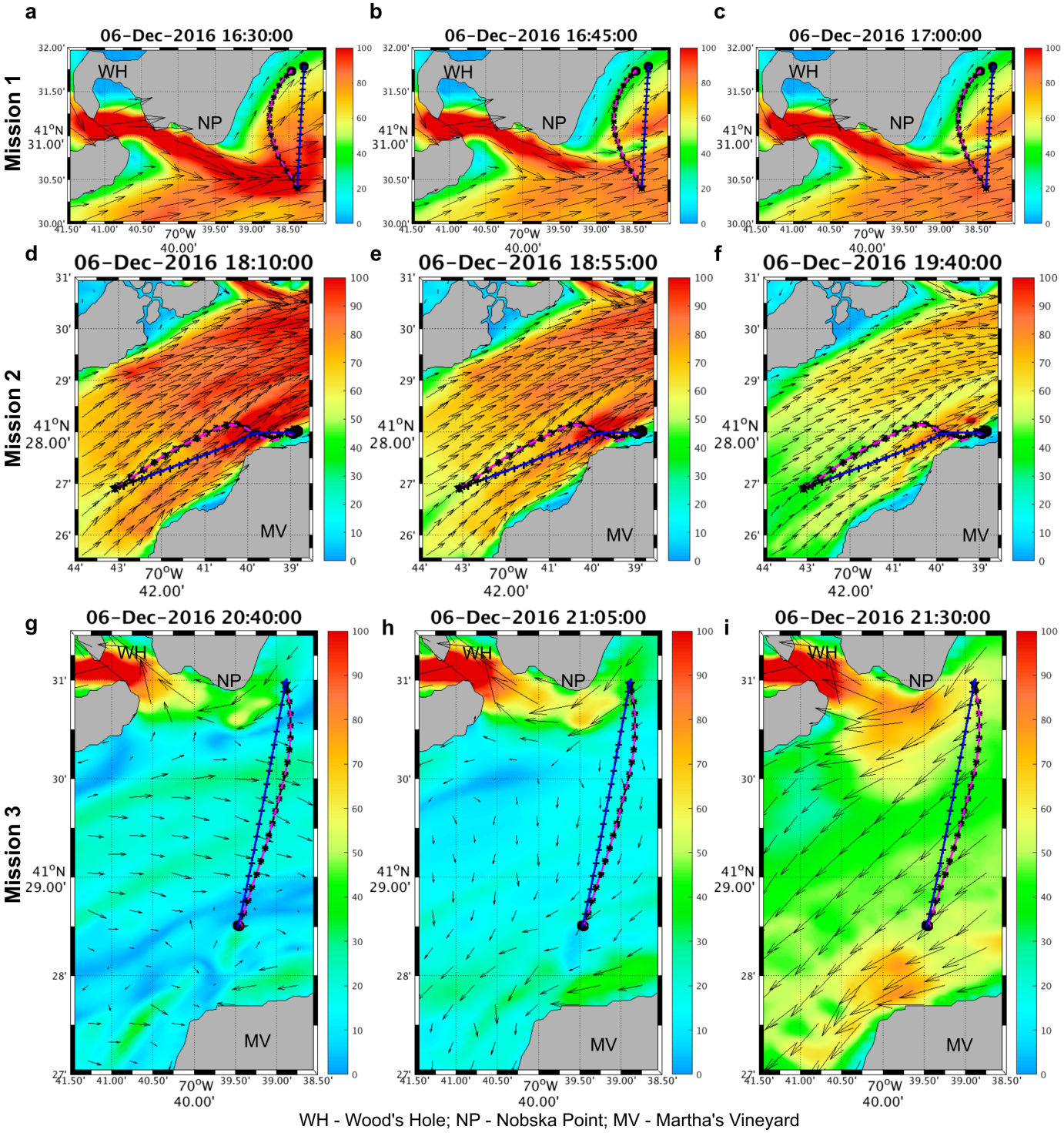

Fig. 12. *Time-Optimal and Straight-Line Paths, as forecast and as realized for the three Missions on 06 Dec 2016. Paths are overlaid on snapshot forecast current velocity vectors and colored magnitude, all at 3 m depth. For each mission, we show the forecast time-optimal way-points ('*' markers) and forecast straight-line way-points ('+' markers) as well as the actual time-optimal path (magenta dashed line) and actual straight-line path (blue dotted line) that were completed by the two AUVs.*

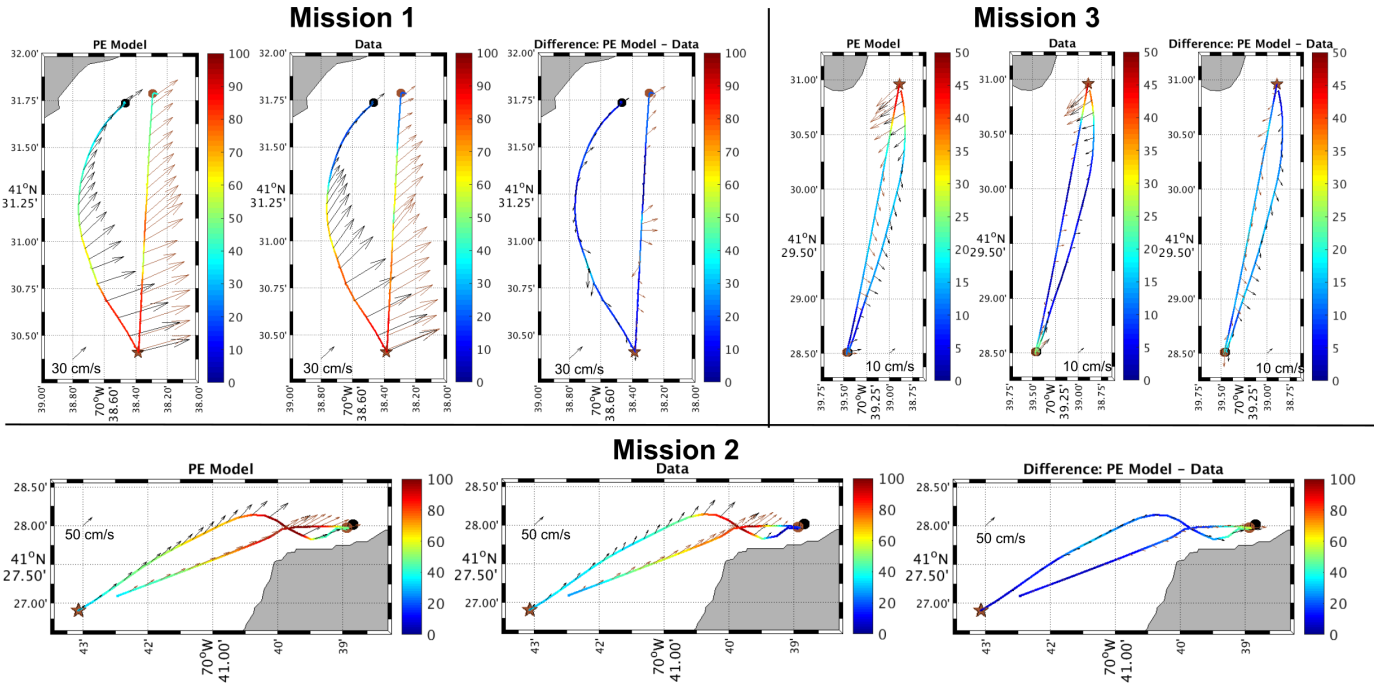

Fig. 13. *Comparison of currents forecast by our MSEAS PE modeling system and measured by the AUV on 06 Dec 2016:* Same as Fig. 8 but for the sea exercise on 06 Dec. 2016.

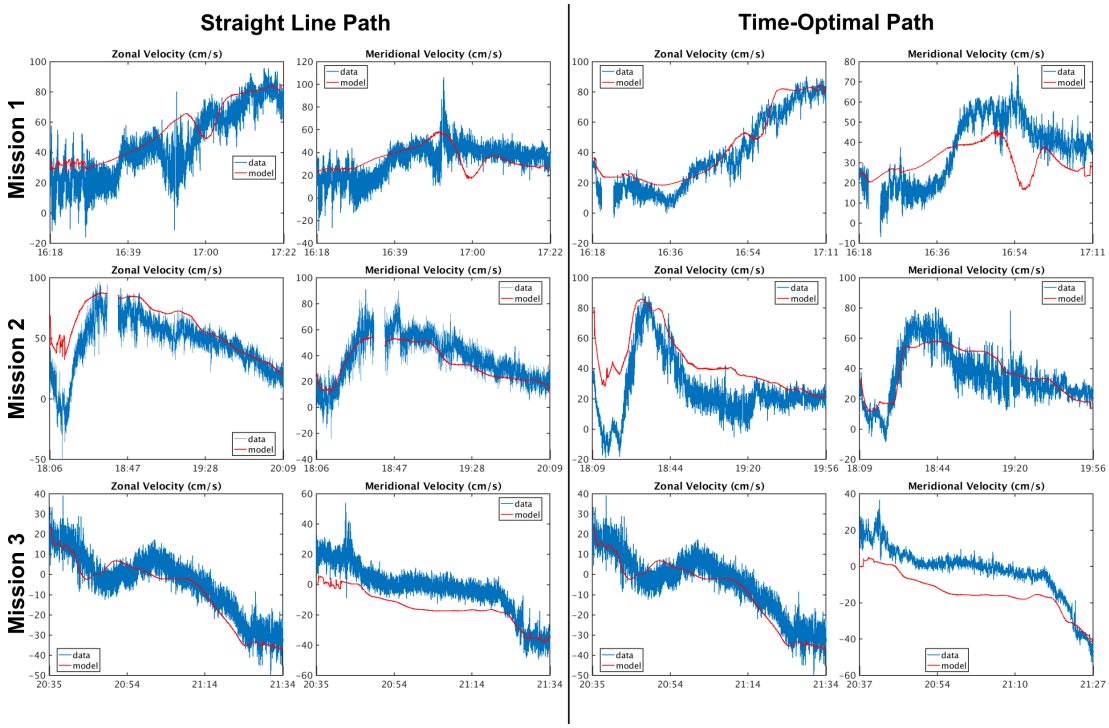

Fig. 14. *Time-series comparison of zonal and meridional components of the currents forecast by our MSEAS modeling system and measured by the AUV on 06 Dec 2016:* Same as Fig. 9 but for the sea exercise on 06 Dec. 2016.

VI. Conclusion

These exercises were the first sea tests of our fundamental time-optimal path planning theory and software. The ocean forecasts from our MSEAS primitive-equation modeling system in the Buzzards Bay and Vineyard Sound Regions had significant skill. The time-optimal path forecasts were very successful with REMUS 600 AUVs, clearly showing the advantage of using our theory and software to save time and win races, even when currents and geometric constraints are complex. We completed some improvements to our path planning software that led to faster computations and data management, and rapid transfer of the paths information to the vehicles. Overall, some of the path computation took less than 10 seconds to complete and be transferred. The results open a new era of optimal AUV missions. The data collected during these missions have also been used to learn AUV characteristics and power consumption [24]. In the future, we would test our theory and equations for energy-optimal planning [4], stochastic time-optimal path planning [25], coordination-optimal planning [6] and adaptive sampling in real-time tests [26], [27] with real AUVs.

Acknowledgment

The authors would like to thank the captain and crew of the *R/V Discovery*. We thank the members of our MSEAS group for useful discussions. We are grateful for the research support and guidance from the Technology and Contracts Office at MIT Lincoln Laboratory. We also thank the Office of Naval Research (ONR) for research support under grants N00014-14-1-0476 (Science of Autonomy - LEARNS) and N00014-15-1-2616 (NASCar-OPS) to the Massachusetts Institute of Technology (MIT). We also thank the MIT-Tata Center Program for the Fellowship support of DNS.

References

[1] J. G. Bellingham and K. Rajan, "Robotics in remote and hostile environments," *Science*, vol. 318, no. 5853, pp. 1098–1102, 2007.

[2] J. Nicholson and A. Healey, "The present state of autonomous underwater vehicle (auv) applications and technologies," *Marine Technology Society Journal*, vol. 42, no. 1, pp. 44–51, 2008.

[3] T. Lolla, P. F. J. Lermusiaux, M. P. Ueckermann, and P. J. Haley, Jr., "Time-optimal path planning in dynamic flows using level set equations: Theory and schemes," *Ocean Dynamics*, vol. 64, no. 10, pp. 1373–1397, 2014.

[4] D. N. Subramani and P. F. J. Lermusiaux, "Energy-optimal path planning by stochastic dynamically orthogonal level-set optimization," *Ocean Modeling*, vol. 100, pp. 57–77, 2016.

[5] T. Lolla, P. J. Haley, Jr., and P. F. J. Lermusiaux, "Time-optimal path planning in dynamic flows using level set equations: Realistic applications," *Ocean Dynamics*, vol. 64, no. 10, pp. 1399–1417, 2014.

[6] ——, "Path planning in multiscale ocean flows: coordination and dynamic obstacles," *Ocean Modelling*, vol. 94, pp. 46–66, 2015.

[7] D. N. Subramani, P. J. H. Jr., and P. F. J. Lermusiaux, "Energy-optimal path planning in the coastal ocean," *Journal of Geophysical Research: Oceans*, 2017, in press.

[8] S. Kemna, M. J. Hamilton, D. T. Hughes, and K. D. LePage, "Adaptive autonomous underwater vehicles for littoral surveillance," *Intelligent service robotics*, vol. 4, no. 4, pp. 245–258, 2011.

[9] S. R. Ramp, R. E. Davis, N. E. Leonard, I. Shulman, Y. Chao, A. R. Robinson, J. Marsden, P. F. J. Lermusiaux, D. M. Fratantoni, J. D. Paduan, F. P. Chavez, F. L. Bahr, S. Liang, W. Leslie, and Z. Li, "Preparing to predict: The second Autonomous Ocean Sampling Network (AOSN-II) experiment in the Monterey Bay," *Deep Sea Research Part II: Topical Studies in Oceanography*, vol. 56, no. 3–5, pp. 68–86, Feb. 2009, doi:10.1016/j.dsr2.2008.08.013.

[10] P. J. Haley, Jr., P. F. J. Lermusiaux, A. R. Robinson, W. G. Leslie, O. Logoutov, G. Cossarini, X. S. Liang, P. Moreno, S. R. Ramp, J. D. Doyle, J. Bellingham, F. Chavez, and S. Johnston, "Forecasting and reanalysis in the Monterey Bay/California Current region for the Autonomous Ocean Sampling Network-II experiment," *Deep Sea Research Part II: Topical Studies in Oceanography*, vol. 56, no. 3–5, pp. 127–148, Feb. 2009, doi:10.1016/j.dsr2.2008.08.010.

[11] M. Michini, M. A. Hsieh, E. Forgoston, and I. B. Schwartz, "Robotic tracking of coherent structures in flows," *IEEE Transactions on Robotics*, vol. 30, no. 3, pp. 593–603, 2014.

[12] A. Alvarez, A. Caiti, and R. Onken, "Evolutionary path planning for autonomous underwater vehicles in a variable ocean," *IEEE Journal of Oceanic Engineering*, vol. 29, no. 2, pp. 418–429, 2004.

[13] J. Witt and M. Dunbabin, "Go with the flow: Optimal auv path planning in coastal environments," in *Proceedings of Australasian Conference on Robotics and Automation*, J. Kim and R. Mahony, Eds., December 2008, pp. 86–94.

[14] B. Garau, M. Bonet, A. Alvarez, S. Ruiz, A. Pascual *et al.*, "Path planning for autonomous underwater vehicles in realistic oceanic current fields: Application to gliders in the western mediterranean sea," *Journal of Maritime Research*, vol. 6, no. 2, pp. 5–22, 2009.

[15] P. J. Haley, Jr. and P. F. J. Lermusiaux, "Multiscale two-way embedding schemes for free-surface primitive equations in the "Multidisciplinary Simulation, Estimation and Assimilation System"," *Ocean Dynamics*, vol. 60, no. 6, pp. 1497–1537, Dec. 2010.

[16] P. J. Haley, Jr., A. Agarwal, and P. F. J. Lermusiaux, "Optimizing velocities and transports for complex coastal regions and archipelagos," *Ocean Modeling*, vol. 89, pp. 1–28, 2015.

[17] D. L. Rudnick, R. E. Davis, C. C. Eriksen, D. M. Fratantoni, and M. J. Perry, "Underwater gliders for ocean research," *Marine Technology Society Journal*, vol. 38, no. 2, pp. 73–84, 2004.

[18] R. P. Stokey, A. Roup, C. von Alt, B. Allen, N. Forrester, T. Austin, R. Goldsborough, M. Purcell, F. Jaffre, G. Packard *et al.*, "Development of the remus 600 autonomous underwater vehicle," in *OCEANS, 2005. Proceedings of MTS/IEEE*. IEEE, 2005, pp. 1301–1304.

[19] "REMUS 600," http://www.whoi.edu/main/remus600, [Online; accessed 14-April-2017].

[20] "Autonomous Underwater Vehicle, REMUS 600," https://www.km.kongsberg.com/ks/web/nokbg0240.nsf/AllWeb/F0437252E45256BDC12574AD004BDD4A?OpenDocument, [Online; accessed 14-April-2017].

[21] G. D. Egbert and S. Y. Erofeeva, "Efficient inverse modeling of barotropic ocean tides," *Journal of Atmospheric and Oceanic Technology*, vol. 19, no. 2, pp. 183–204, 2002.

[22] O. G. Logutov and P. F. J. Lermusiaux, "Inverse barotropic tidal estimation for regional ocean applications," *Ocean Modelling*, vol. 25, no. 1–2, pp. 17–34, 2008. [Online]. Available: http://www.sciencedirect.com/science/article/pii/S1463500308000851

[23] P. J. Haley, Jr., P. F. J. Lermusiaux, and S. Kelly, "Multiscale dynamic relaxation and sponge open boundary conditions." Department of Mechanical Engineering, Massachusetts Institute of Technology, Cambridge, MA, USA, MSEAS Report, 2015.

[24] J. Edwards, J. Smith, A. Girard, D. Wickman, D. N. Subramani, C. S. Kulkarni, J. P. J. Haley, C. Mirabito, S. Jana, and P. F. J. Lermusiaux, "Data-driven learning and modeling of AUV operational characteristics for optimal path planning," in *Oceans '17 MTS/IEEE Conference*, Aberdeen, Jun. 2017, in Press.

[25] D. N. Subramani, Q. J. Wei, and P. F. J. Lermusiaux, "Stochastic time-optimal path planning in uncertain dynamic flows," *Ocean Dynamics*, 2017, to be submitted.

[26] P. F. J. Lermusiaux, "Adaptive modeling, adaptive data assimilation and adaptive sampling," *Physica D: Nonlinear Phenomena*, vol. 230, no. 1, pp. 172–196, 2007.

[27] K. D. Heaney, P. F. J. Lermusiaux, T. F. Duda, and P. J. Haley, Jr., "Validation of genetic algorithm based optimal sampling for ocean data assimilation," *Ocean Dynamics*, vol. 66, pp. 1209–1229, 2016.